

Primordial features and Planck polarization

Dhiraj Kumar Hazra,^a Arman Shafieloo,^b George F. Smoot,^{a,c,d,e}
Alexei A. Starobinsky^{f,g}

^aLaboratoire APC-PCCP, Université Paris Diderot, 10, rue Alice Domon et Leonie Duquet, 75205 Paris Cedex 13, France

^bUniversity of Science and Technology, Daejeon 34113, Korea

^cUniversité Sorbonne Paris Cité, 75013 France

^dInstitute for Advanced Study, Hong Kong University of Science and Technology, Clear Water Bay, Kowloon, Hong Kong

^ePhysics Department and Lawrence Berkeley National Laboratory, University of California, Berkeley, CA 94720, USA

^fLandau Institute for Theoretical Physics RAS, Moscow, 119334, Russian Federation

^gKazan Federal University, Kazan 420008, Republic of Tatarstan, Russian Federation

E-mail: dhiraj.kumar.hazra@apc.univ-paris7.fr, shafieloo@kasi.re.kr,
gfsmoot@lbl.gov, alstar@landau.ac.ru

Abstract. With the Planck 2015 Cosmic Microwave Background (CMB) temperature and polarization data, we examine possibility of having features in the primordial power spectrum (PPS). We revisit the Wiggly Whipped Inflation (WWI) framework and demonstrate how generation of some particular primordial features can improve the fit to Planck data. WWI potential allows the scalar field to transit from a steeper potential to a nearly flat potential through a discontinuity either in potential or in its derivatives. Using Planck 2015 data, we constrain the primordial features in the context of Wiggly Whipped Inflation and present the features that are supported both by temperature and polarization. WWI model provides upto $\sim 12 - 14$ improvement in χ^2 fit to the data with respect to the best fit power law model considering combined temperature and polarization data from Planck and B-mode polarization data from BICEP and Planck dust map. We use 2-4 extra parameters in the WWI model compared to the featureless strict slow roll inflaton potential. WWI offers a wide variety of features in the primordial power spectra incorporating a number of models discussed in the literature that can address localized and non-local features in the temperature and polarization angular power spectrum. We find that the difference between the temperature and polarization data in constraining background cosmological parameters such as baryon density, cold dark matter density are reduced to a good extent if we use primordial power spectra from WWI. We also discuss the extent of bispectra obtained from the best potentials in arbitrary triangular configurations using the BI-spectra and Non-Gaussianity Operator (BINGO).

Contents

1	Introduction	1
2	Wiggly Whipped Inflationary Scenario	2
2.1	The potentials	3
2.2	Classes of features in WWI	4
3	Essential numerical details	6
4	Results and discussions	7
4.1	Primordial scalar perturbation power spectrum	7
4.2	Best fit results	8
4.3	Change in the parameter constraints	13
4.4	Non-Gaussianity	15
5	Conclusions	17

1 Introduction

While viable inflationary models of the early Universe have succeeded in the quantitative description of the main, smooth part of the primordial power spectrum (PPS) of scalar (adiabatic density) perturbations $P_S(k)$, and have even predicted its observed slope $n_s(k)$ for some simplest variants of them, the complete shape of the primordial power spectra has not been established beyond doubt. It is natural to expect small corrections to this smooth behavior which reflect new and subtle physical effects occurring during inflation. Indeed, some relatively small features ($\lesssim 10\%$) have already been noticed in the low- ℓ ($\ell \lesssim 40$) multipole region of CMB fluctuations since WMAP, which may result from tiny localized features in the PPS.

With the release of the new Planck temperature and polarization data [1–3], we are now in a unique position to examine the existence of primordial features in the scalar perturbations to a great precision over a wide range of cosmological scales. We had indication of primordial features in all releases of WMAP temperature data [4–7] and Planck 2013–2015 temperature data [8, 9] and we have knowledge about the location and the types of the features from reconstructions of the primordial power spectrum. Inflaton potentials, addressing the primordial features were proposed along the lines, that provided notable, if not significant, improvement in fit compared to the standard power law primordial spectrum from slow roll inflation. A large scale scalar suppression, a dip near $2 \times 10^{-3} \text{Mpc}^{-1}$, oscillations around 0.02Mpc^{-1} and around 0.06Mpc^{-1} wavenumbers, are few notable features from Planck 2013 temperature anisotropy data [10]. Interestingly, the necessity of the large scale suppression of scalar power became significant when BICEP2 B-mode signal were considered primordial [11, 12]. The effect of tensor perturbation at the large scale temperature anisotropies aggravated (at more than 3σ level [13]) the already existing issue of lack of low-multipole power of temperature anisotropies (1σ support of power suppression from Planck 2013 TT data) [14]. We proposed Whipped Inflation (WI) [15] and Wiggly Whipped Inflation (WWI) [16] that could address all the above mentioned issues with the primordial

power spectra and provided significant improvement in fit compared to canonical slow roll models of inflation. Today, with the BICEP2 signal being consistent to dust polarization, one can anticipate a dramatic decrease in significance of the large scale suppression. Also the large magnitude of quadratic potential, used in WI and WWI makes it unsuitable for recent BICEP2/KECK-Planck joint constraints on the primordial B-modes (tensor-to-scalar ratio $r < 0.07$ at 95% confidence level [17, 18]). However, note that the significance of the Wiggles in the WWI are not altered by change in the BICEP2 results since they were designed to address features in Planck temperature data.

Since we now have tighter constraints in background and primordial cosmology from the new temperature and polarization data, it is important to revisit the status of features in the light of new data. It is also appropriate to modify the WWI potential that can satisfy present bounds on B-mode and dust polarization. If temperature and polarization votes for similar features it definitely shall increase its likelihood, hence equipped with Planck polarization data covering the largest cosmological scales it is definitely worth having a joint constraints on features. Change in constraints on the background cosmological parameters in the presence of features is another aspect that should be investigated. In this paper, we explore the above mentioned. It is clearly not possible to examine every primordial feature within a single framework of potential. However, we show that our WWI potential is capable of producing a large variety of features that are discussed in the literature, which makes it extremely efficient to hunt different types of features required by different datasets in the same framework.

The paper is organized as follows: In section 2 we review the WWI potential in its old and modified form. We demonstrate to what extent WWI potential can offer a variety of features in the PPS. In section 3 we discuss the methodology, *i.e.* a brief outline of our numerical analysis. We provide our best fit results and constraints on the model in section 4. We also present the bispectra from the best fits to the data in arbitrary triangular configurations of wavenumbers. We conclude in section 5.

2 Wiggly Whipped Inflationary Scenario

The basic construction of the Wiggly Whipped Inflation potential followed the form :

$$V(\phi) = V_S + \gamma V_R, \quad (2.1)$$

where, V_R represents the part of the potential that introduces a moderate fast roll and V_S is chosen to be nearly flat, allowing a strict slow roll. Here, γ determines how fast the inflaton starts rolling initially and in a way it determines the extent of deviation from slow-roll and thereby deviations from featureless PPS. Similar types of phase transition potential have been discussed widely in the literature [19–25]. V_R contains a Theta step function ensuring the termination of moderate fast roll after certain field value. Thereafter the scalar field emerges to the strict slow roll regime. In this framework, the potential and/or its derivatives can contain discontinuities.

The WWI model was introduced in [16] in order to address two major issues. Firstly with the BICEP2 B-mode signal, assuming to be primordial, we ruled out the power law form of scalar power spectrum with more than 3σ confidence [13]. We needed a strong suppression of scalar power at large scales and at the same time large tensors with low non-Gaussianities.

Whipped inflation [15] that simply uses a smooth transition from a moderate fast roll potential (V_R) to a strict slow roll inflation (V_S , assumed to be a quadratic potential) meets all the above criteria. On top of that in order to address the primordial features indicated by Planck temperature anisotropies, we introduced a discontinuity in the potential (or in its derivatives, keeping a continuous potential) at the transition which provided significant improvement in likelihood to the Planck and assumed primordial B-mode from BICEP2 compared to the power law PPS. The scalar PPS, containing a Whipped shaped tail at large scales and Wiggles (oscillatory behavior), the Inflaton potential was referred as Wiggly Whipped Inflation potential. The BICEP-2 B-mode signal being consistent to dust polarization, do not favor a large field quadratic model since it produce large primordial B-modes. At the same time the significance of the requirement of a large scale scalar suppression reduces. However, since we now have polarization data from Planck, it is important to test the WWI model features with the new datasets. In this paper we use the WWI potential with a modification to the slow roll part of the potential.

2.1 The potentials

We use the WWI model in a modified form. Since BICEP2 B-mode signal is consistent with dust polarization power spectra from Planck, a model with high tensor-to-scalar ratio ($r \sim 0.2$) is not supported by the data anymore. Hence we use a lower potential in the slow roll part. We use two different classes of WWI potential here, in the first case we have discontinuity in the potential while in the second case the potential is continuous with a discontinuity in its slope. Both of them belong to the WWI form, but to distinguish them conveniently, we refer the first potential as WWI and the second as WWI'. Note that since the tensor perturbations depends on the scale of the potential, in order to get a lower tensors we need to scale down the potential. Here, our basic structure of the potential remains same and provided below in Eq. 2.2

$$V(\phi) = V_i \left(1 - \left(\frac{\phi}{\mu} \right)^p \right) + \Theta(\phi_T - \phi) \gamma V_i ((\phi_T - \phi)^q + \phi_{01}^q) \quad (2.2)$$

The slow roll potential $V_i \left(1 - \left(\frac{\phi}{\mu} \right)^p \right)$ depends on 2 parameters, namely the potential at $\phi = 0$ (V_i) and μ . The spectral index (n_s) and the tensor-to-scalar ratio (r) of the PPS generated at the end of inflation depends on μ and the power p . We chose the value $p = 4$ and $\mu = 15M_{\text{PL}}$ such that $n_s \sim 0.96$ and $r \sim \mathcal{O}(10^{-2})$ (as in [28, 29]). The fast roll part of the potential remains identical to the original WWI potential. ϕ_T denotes the field value where the transition from the moderate fast-roll to complete slow-roll occurs. ϕ_{01} is the extent of discontinuity and γ is the slope that provides the deviation of slow-roll at the onset of inflation. $\phi_{01} = 0$ reduces the potential to Whipped Inflation form where the potential and its derivatives are continuous upto $(q - 1)$ 'th derivatives. The Heaviside Theta function $\Theta(\phi_T - \phi)$ appearing in the potential can be modeled by a Tanh step $(1 + \tanh[(\phi - \phi_T)/\Delta])$ or Error function step $(1 + \text{erf}[(\phi - \phi_T)/\Delta])$ and the width of the step (Δ) can be used as a free parameter. The scalar field starts from the bottom of a quadratic potential (for $q = 2$) and transits to the strict slow roll potential at $\phi = \phi_T$. The initial deviation from slow-roll introduces a whip shaped suppression of power at large and intermediate scales in the PPS. $\phi_{01} > 0$ creates a temporary sharp departure from slow-roll and generates wiggly features locally or extending a large range in cosmological scales depending on the sharpness

of transition, Δ . Hereafter, throughout the paper, with WWI, we shall refer to the potential in Eq. 2.2.

Using similar formalism, we investigate another potential that is continuous, but has discontinuities in its derivatives. The potential can be expressed as,

$$V(\phi) = \Theta(\phi_T - \phi)V_i(1 - \exp[-\alpha\kappa\phi]) + \Theta(\phi - \phi_T)V_{ii}(1 - \exp[-\alpha\kappa(\phi - \phi_{01})]) \quad (2.3)$$

Here $V_i(1 - \exp[-\alpha\kappa\phi])$ is the slow roll part of the potential which is present at $\phi \leq \phi_T$ and for higher field values, $V_{ii}(1 - \exp[-\alpha\kappa(\phi - \phi_{01})])$ represents the moderate fast roll part. Note that we have used the α -attractor potential [26] to construct a model providing deviations from slow roll. V_{ii} is related to V_i by our demand of continuity in the potential. $\kappa^2 = 8\pi G$ (which we equate to 1 in our convention). α denotes the slope of the potential and we have fixed it to be $\sqrt{2/3}$ that corresponds to the $R + R^2$ inflationary model [27] in the Einstein frame. It produces a tensor-to-scalar ratio of $\sim 4 \times 10^{-3}$ for the slow roll part of the spectra. Hence ϕ_T and ϕ_{01} are the only two extra parameters in our potential compared to the strict slow roll part of the potential. Note that this potential can also have a discontinuity if V_{ii} is treated as a free parameter, but since we have already incorporated potential discontinuities in Eq. 2.2, in Eq. 2.3 we fix V_{ii} through the continuity. We denote this potential with WWI' to indicate that the potential has a discontinuity only in its derivatives. The primordial feature generated from WWI' is very similar to the original Starobinsky-1992 model [19] but here, the scalar PPS has the asymptotic value of $n_s \sim 0.96$.

2.2 Classes of features in WWI

CMB angular power spectrum data since WMAP have indicated hints towards possible deviations from the standard power law PPS. Reconstructions of the PPS directly from the angular power spectrum data [10, 30] have been very useful in order to highlight different locations and types of these deviations (features) in the PPS. Using Planck 2013 data, it has been demonstrated [10] that the temperature anisotropy power spectrum indicates a suppression at large scale power, few localized oscillations around $\ell \sim 22$, $\ell \sim 250 - 300$ and $\ell \sim 750 - 850$. Non-standard inflationary models have been proposed in order to generate different kinds of features in the PPS. Below we enlist a non-exhaustive discussion of primordial features.

1. Large scale power suppression : The primordial power spectrum with a large scale suppression can be modeled by a broken power law with different spectral index at different scales, or a Tanh step (both these types have been discussed in [14]) or an exponential cutoff [31]. These types of features are generated when the scalar field changes its kinetic energy in the first few *e-folds*. Starting from Starobinsky-1992 model [19], different models [15, 24, 32] have been proposed that offers such scenarios. A brief halt in inflation caused by an inflection point [33] in the potential can produce a sharp cut-off at the large scale primordial power. Open inflation [20, 21], radiation dominated epoch prior to inflation [34] also known to provide such class of spectra. In Fig. 1 we plot such type of spectra (in the top left) that are obtained from WWI (Eq. 2.2). Note that in these cases, large value of the parameter γ allows an initial faster roll and hence provide a cutoff at the large-intermediate scales.

2. Localized oscillation : Near multipoles $\ell \sim 22$ and $\ell \sim 40$ a dip and a bump *w.r.t.* the angular power spectra from power law were noticed since WMAP data. This feature patterns in a localized scale and requires wiggles in the PPS only at certain wavenumbers, keeping the other part of the PPS nearly scale invariant. Presence of a *step in the inflaton*

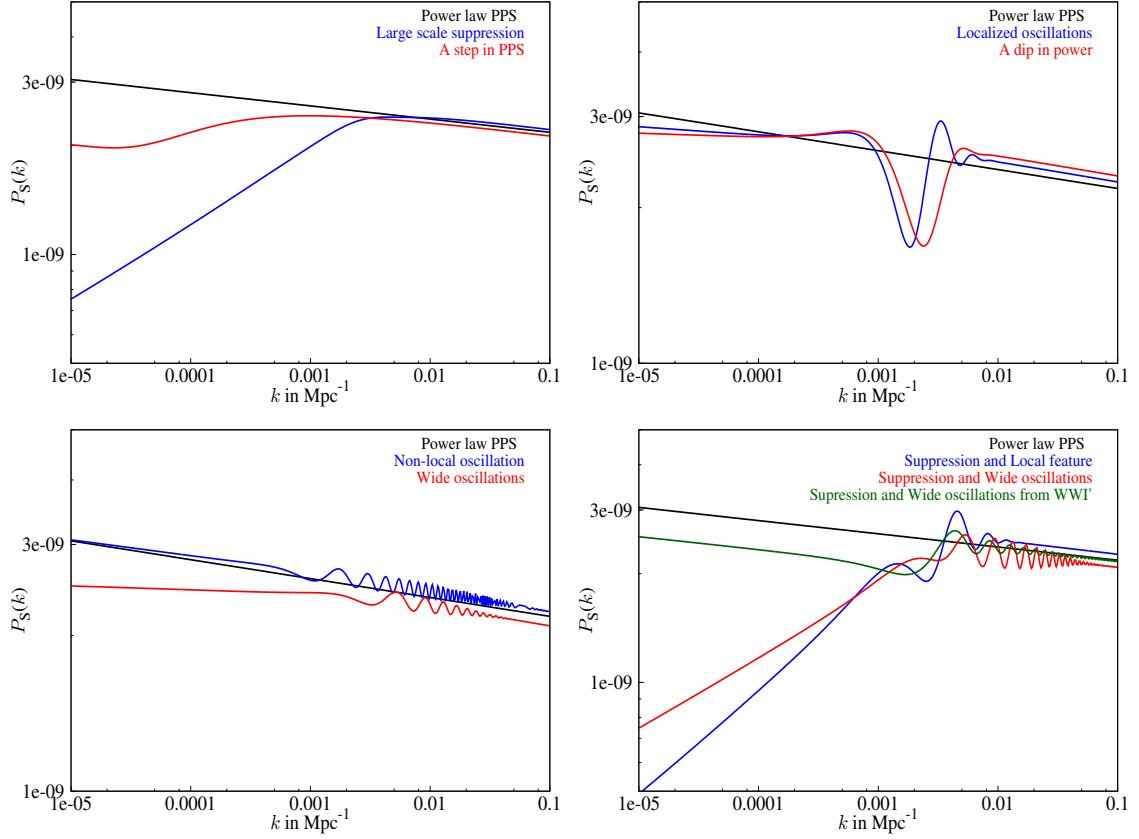


Figure 1. [Top left] : PPS with suppression at large scale scalar power. We show that WWI (Eq. 2.2) can generate a exponential cutoff (blue) type PPS and also a PPS with a form of a step (red). [Top right] Here WWI produces localized oscillations. Note that a dip or a period of oscillation around 0.002Mpc^{-1} improves the fit to the data near multipole $\ell = 22$. [Bottom left] Wide features and non-local oscillations. The angular power spectra are affected for a wide range of multipoles. [Bottom right] We provide a combination of different features. The large range of features that are addressed by WWI models, makes WWI a suitable candidate to search for generic features in the primordial power spectrum. A typical step like suppression, accompanied by wiggles in the PPS is generated by the WWI' (Eq. 2.3) and is plotted here as well.

potential [29, 35] provides a momentary departure from the slow roll and generate localized oscillations in the PPS. It has been shown that around $k \sim 0.002\text{Mpc}^{-1}$ and $k \sim 0.004\text{Mpc}^{-1}$, a period of oscillation can improve the match to the data compared to the power law model. However, because of uncertainties owing to the cosmic variance, the existence of such large scale feature have never been (possibly never will be) established beyond doubt. Top right of Fig. 1 shows similar features from WWI. Here, γ is small such that the fast roll part is not significant and we get nearly same tilt both at large and small scales. However, due to ϕ_{01} , the field goes through a momentary departure from slow roll and generates localized oscillations.

3. Non-local features : Features that extend over a wide range of cosmological scales are termed as non-local features. A slow roll potential modulated with sinusoidal oscillations or presence of discontinuities in the potential and its derivatives give rise to such non local features. Effects of oscillations in the inflation potential [36] have been studied before with WMAP and Planck datasets. In [16] we discussed the features generated by the WWI model

and demonstrated that non-local features in the WWI can provide similar improvement in fit as local feature models. Fig. 1, bottom left plot demonstrates such features from WWI. Here, γ and ϕ_{01} are small and hence we do not observe any cutoff and the amplitude of the features are small as well. However, in these models $\Delta \ll 1$ and hence the field experience a sharp transition and a wide range of modes that leaves Hubble scale after the epoch of transition imprints oscillations in the PPS.

Wiggly Whipped Inflation, interestingly, is capable of generating all the above features and hence, we present it as the model offering a wide variety of scenarios, within the framework of canonical scalar field Lagrangian. Fig. 1 bottom right plot represent two such PPS that offers the aforementioned classes of features in combination, all arising from the same potential. Note that in the same plot we present the feature obtained from WWI'. The discontinuity in the derivative of the potential leads to a power spectrum that offers a step shaped suppression at larger scales, followed by wiggles at the smaller scales. In this case, the amplitude of oscillations decrease as we probe smaller scales.

3 Essential numerical details

We use the publicly available code BI-spectra and Non-Gaussianity Operator, BINGO [37, 38] to generate the power spectra and the bispectra from WWI and WWI'. We solve the background equation using a initial value of the field ϕ to ensure enough (~ 70 *e-folds*) inflation. $d\phi/dt$ is fixed assuming initial slow-roll condition ($3Hd\phi/dt = -dV(\phi)/d\phi$). Whenever necessary, we model the Theta function discontinuities in the potential and delta function in its derivatives with a Tanh step and its derivatives respectively. Note that other representations of Theta function and delta function can also be used in this context. Following standard methodology we fix the initial scale factor by assuming the $k = 0.05\text{Mpc}^{-1}$ mode leaves the Hubble radius 50 *e-folds* before the end of inflation.

We use publicly available CAMB [39, 40] and COSMOMC [41, 42] in order to calculate the angular power spectra from our models and compare them with the data. Note that, we modify CAMB in order to use BINGO to calculate the primordial scalar and tensor power spectra. Along with the baryon density ($\Omega_b h^2$), cold dark matter density ($\Omega_{\text{CDM}} h^2$), the ratio of the sound horizon to the angular diameter distance at decoupling (θ) and the optical depth (τ), we allow the WWI parameters, namely V_i , γ , ϕ_{01} and ϕ_T to vary. We treat the WWI parameters as semi slow-parameters (like the amplitude A_S , spectral index n_S , tensor-to-scalar ratio (r) in case of power law PPS). Note that we also allow the width (Δ) of the Theta function to vary along with other potential parameters. For WWI' we treat V_i and ϕ_T and ϕ_{01} as potential variables. In order to obtain the best fits we use Powell's BOBYQA (Bound Optimization BY Quadratic Approximation) method of iterative minimization [43]. Since WWI offers a wide variety of features, it is extremely difficult to converge to a global minima starting from a particular region of potential parameter space. Most of the times the method settles to a local minima which represent particular features that provide a better fit to a subset of the complete Planck datasets. We approach this problem in 2 steps. First, we use temperature, polarization datasets separately and in combination so that we can identify the primordial features supported by the individual and complete Planck and BICEP2/KECK datasets. Secondly, in each of the above cases we perform MCMC analyses and locate distinguishable features that provide better fit to the corresponding datasets compared to power law model. We use the WWI potential parameters and corresponding

background cosmological parameters corresponding to the located features and use them as starting points of BOBYQA minimization. Using this rigorous search, we are able to obtain the local minima and possibly the global minima for the individual and complete datasets.

We use CMB temperature and polarization data from Planck-2015 public release datasets and likelihoods. In order to understand the necessity of features in the PPS indicated from temperature and polarization data, we use the temperature and polarization likelihood from Planck separately and in combination. For high- ℓ temperature and polarization data, we use the Plik likelihood that covers the multipoles $\ell = 30 - 2508$ for TT and $30 - 1996$ for TE and EE.

For the low- ℓ part of the spectra ($\ell = 2 - 29$) we use 2 different likelihoods in different cases. When we use only TT likelihood at high- ℓ , we use commander based likelihood for low- ℓ TT. In this paper we denote this likelihood as lowT. We use lowTEB likelihood at low- ℓ whenever we use EE data at high- ℓ or temperature and polarization likelihood in combination. The low- ℓ polarization uses the 70GHz LFI full mission (except second and fourth surveys) data. We use TTTEEE likelihood and use TT + TE + EE likelihood at high- ℓ to track down the improvement in likelihood (compared to the power law model of the PPS) in complete and individual datasets. The high- ℓ likelihood uses 100, 143 and 217 GHz half mission maps. Throughout our analyses, we have varied all the required nuisance and calibration parameters for the corresponding likelihoods. We also use priors on nuisance and calibration parameters as have been discussed in [1, 44].

We use BICEP2-Keck likelihood from the joint BICEP2/Keck and Planck analysis (BKP) [17]. In our analyses we use 5 bandpowers in the range $\ell = 20 - 200$, from 150 GHz band of BICEP2/Keck and 217GHz and 353GHz bands of Planck. Needless to mention we compute and use the tensor power spectra from the models when we confront the models with BKP datasets.

We use the BINGO-2.0 version in order to evaluate the bispectra in equilateral and arbitrary triangular configurations. We have defined $M_{\text{Pl}}^2 = 1/(8\pi G) = 1$ and used $\hbar = c = 1$ throughout the paper.

4 Results and discussions

We present our results in this section in the following manner. We provide the best fit primordial power spectrum that we obtained from the complete datasets. We tabulate the best likelihood values and the improvement in fit from WWI compared to the power law PPS. Using the best fit values, we compare the best fit angular power spectra of temperature and polarization and their cross-correlations *w.r.t* best fit Planck baseline models. We compare the background parameter constraints from the MCMC analyses against different datasets. Finally, we present the bispectra in equilateral and arbitrary triangular configurations for the best fit models.

4.1 Primordial scalar perturbation power spectrum

We have demonstrated that WWI offers a wide variety of features in the primordial power spectra. When compared against the Planck datasets we locate 4 local minima that provide substantial better fit compared to the power law power spectra. We categorize the local regions of parameter space by their distinct nature of features. We denote them as WWI-[a,b,c,d]. We plot these models in left and middle plots of Fig. 2. Here we should stress that WWI-[a,b,c,d] that are plotted in the figure, in strict sense, are the local minima of

the TTTEEE + lowTEB + BKP combination. WWI-a is actually the global minima of TT + lowT dataset, that turns out to be a local minima of the complete datasets. WWI-c on the other hand, has characteristic wide scale oscillations that provide improvement in fit to the high- ℓ EE data. We search for the local and global minima in other individual and combination of datasets in the vicinity of WWI-[a,b,c,d]. Obviously the best fit parameters will be different when we compare different datasets. However, the broad shape of that particular feature remains similar in all the datasets since the WWI potential parameters do not change significantly. The right plot of the same figure provide best fit PPS from WWI' when compared against T, E and combined datasets.

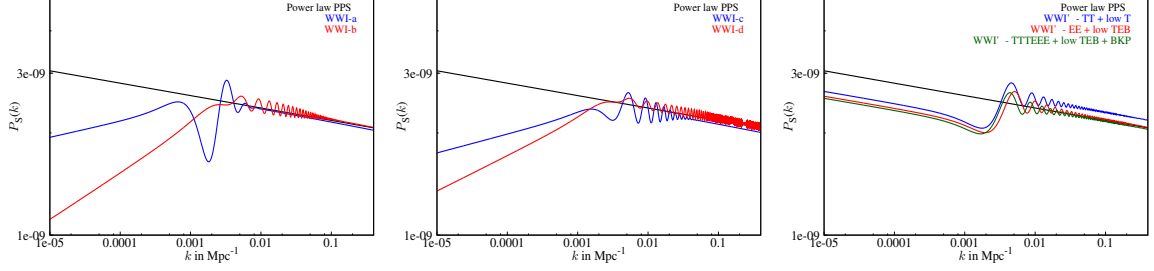


Figure 2. Wiggly Whipped Inflation : Best fit primordial power spectra. Left plot contains the local minima, WWI-[a,b] and the middle plot contains WWI-[c,d] respectively (Eq. 2.2). WWI-a provides $\sim 7 - 8$ improvement in χ^2 fit to temperature only data. Mainly the improvement comes from the large scale power suppression and $\ell \sim 22 - 40$ region. WWI-c provides ~ 10 improvement in χ^2 fit to polarization data. This improvement comes from low- ℓ TEB and high- ℓ E data. WWI-b provides ~ 11 and WWI-d provides $\sim 12 - 14$ improvement to combined temperature and polarization datasets. In this case, most of the improvement comes owing to the inability of baseline model in fitting the temperature and polarization datasets in a combination. The plot at the right contains the WWI' (Eq. 2.3) best fit when compared with T, E and combined datasets. For the combined datasets, WWI' provides nearly 12 improvement in the fit compared to power law best fit.

4.2 Best fit results

In Table 1 we tabulate the best fit $-2 \log [\text{Likelihood}]$ for the WWI-[a,b,c,d], WWI' and the Planck baseline model. Each row block of the table contains the data combination that we used. From top to bottom we provide the analyses for TT + lowT, EE + lowTEB, TTTEEE + lowTEB, TT + TE + EE + lowTEB + BICEP-Keck-Planck dust, TTTEEE + lowTEB + BICEP-Keck-Planck dust. Here we should mention again that the cosmological parameters do change when compared with different combination of datasets. For example WWI-a that is a local minima of TTTEEE + lowTEB (as plotted in Fig. 2) is not *strictly* a local minima of TT + lowT (the position and the amplitude of the features may vary a little). We find with a marginal change in parameter values, a PPS very close in shape to WWI-a, represent the global best fit to TT + lowT datasets. Since Powell's minimizer algorithm converges to a point very close to the parameter space of the starting point in our cases, we searched for the local best fit to TTTEEE + lowTEB + BKP data in the vicinity of the global best fit to TT + lowT data. Hence, WWI-[a,b,c,d] represent a class of resembling PPS that can possibly be a global best fit to a subset of data but in strict sense they are local best fit to the TTTEEE + lowTEB + BKP dataset. However, since WWI' has a unique shaped PPS, in Fig. 2 we plotted the obtained global best fits of TT + lowT, EE + lowTEB and TTTEEE + lowTEB + BKP datasets.

Individual likelihoods comparison						
Individual likelihood	Baseline	WWI-a	WWI-b	WWI-c	WWI-d	WWI'
TT	761.1	762	761.9	762.8	762.8	762.4
lowT	15.4	8.2	13.4	12.1	13	10.2
EE	751.2	748.8	747.2	748.6	750.2	746.8
lowTEB	10493.6	10490	10495.6	10492.4	10495.7	10492.2
TTTEEE	2431.8	2432.7	2422.6	2427.8	2421.7	2426.5
lowTEB	10497.4	10490.8	10495.1	10493.4	10495.3	10492.7
TT	764.5	763.6	762.2	764.4	762.9	762.8
EE	753.9	754.8	750.5	750.8	750.8	751
TE	932	933.4	928.7	929.2	927	928.8
lowTEB	10498.4	10490.4	10495.8	10493.7	10495.6	10492.4
BKP	41.6	42	42	42.6	41.8	42.9
TTTEEE	2431.7	2432.8	2421.4	2426.7	2421	2425.7
lowTEB	10498.5	10490.5	10495.5	10493.6	10495.8	10492.6
BKP	41.6	42	42.7	42	41.9	42.5

Table 1. Best fit parameters for the Wiggly Whipped Inflaton potential. We provide the best fit $-2\ln[\text{Likelihood}]$ for individual datasets for the types of WWI features denoted as WWI-[a,b,c,d], WWI' and that are plotted in Fig 2. Note that while WWI-[a,c] provide local best fits to individual and combined data, WWI-[b,d] seem to capture the global best fit by providing improvement in all datasets (TT, TE, EE) in a combination when compared with power law model. The best fit background, WWI potential and nuisance parameters do indeed change to certain extent in different dataset combinations but the primordial power spectrum remains very similar to the ones plotted in Fig. 2 for all dataset combinations. In case of WWI', note that the similar shaped features (shown in right plot of Fig. 2) are able to address both temperature and polarization data individually and in combinations. We find similar improvement in fit ($\Delta\chi^2 \sim 12$ compared to power law) as in WWI-[b,d] but here only with 2 extra parameters. WWI' also provides the best likelihood to the high- ℓ EE data. We do not provide in the table, the $\mathcal{O}(1)$ improvement in fits from the priors in the nuisance and calibration parameters.

Note that WWI-a provides improvement in likelihood principally for the lowT case. The localized feature similar to step in the inflaton potential around $k \sim 0.002 \text{ Mpc}^{-1}$ ($\ell \sim 22$) along with the large scale power suppression provides around 8 improvement in fit to the lowT and lowTEB data. WWI-a also provide some improvement to the high- ℓ EE data. WWI-c which introduces wiggles in the PPS ranging $k \sim 0.002 - 0.05 \text{ Mpc}^{-1}$ provide a moderate improvement to lowT and lowTEB datasets due to the large scale suppression but fails to capture the $\ell \sim 22$ dip in TT. However the wide wiggles provide a better fit to EE and TE-datasets. WWI-b and WWI-d, though having wiggles in the primordial power spectrum, do not provide better fit to individual temperature or polarization data at high- ℓ but they provide an overall better fit when the complete datasets are compared with. Note that when we combine T and E datasets (TT + TE + EE + lowTEB + BICEP-Keck-Planck dust), the baseline model provide worse fit to TT and EE datasets *w.r.t.* their values when compared individually (TT + lowT and EE + lowTEB). This difference arise because temperature

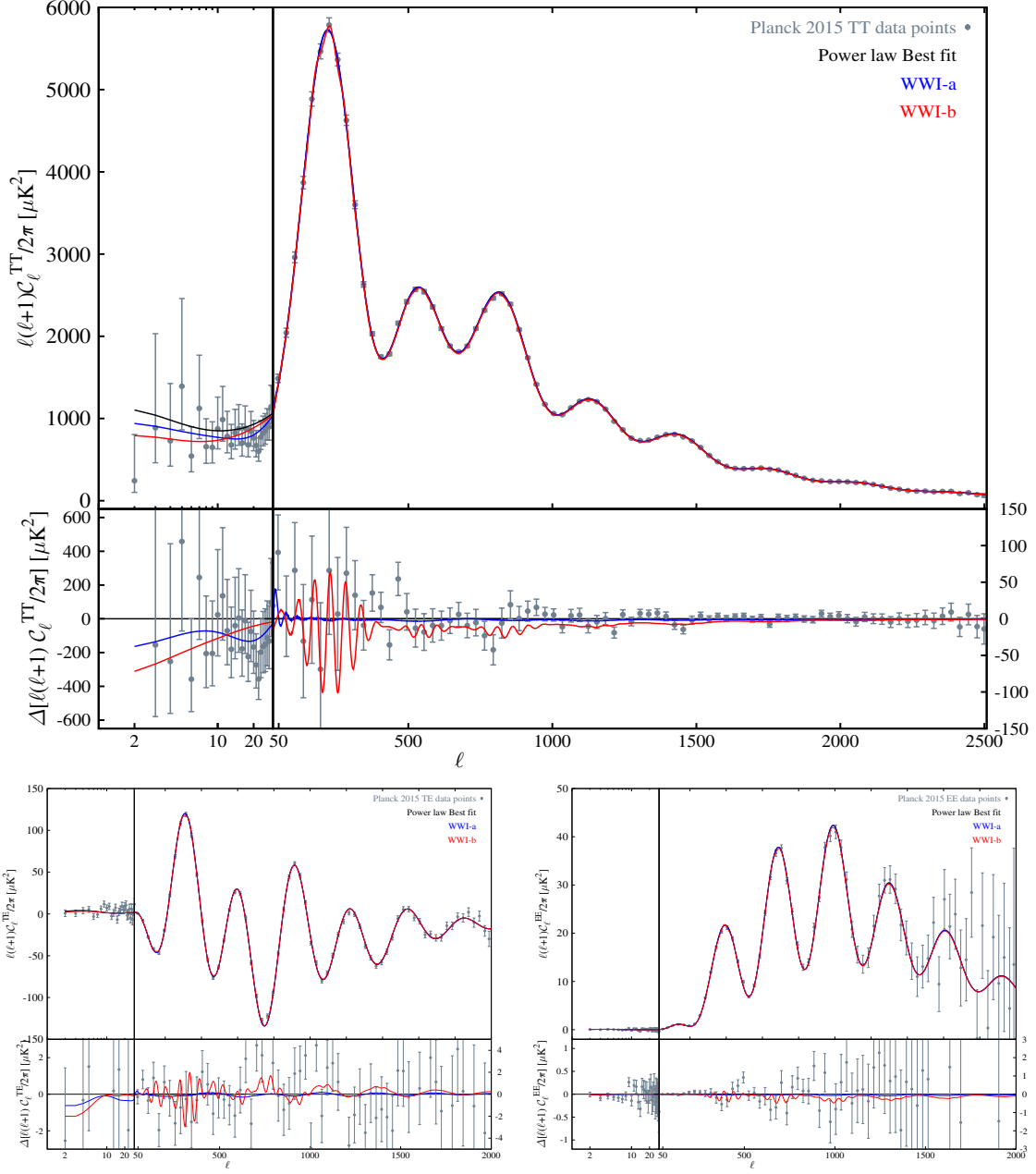


Figure 3. Wiggly Whipped Inflation : Angular power spectra for temperature and polarization anisotropies. Theoretical predictions from WWI-a and WWI-b are provided. These are the best fits to TTTEEE + lowTEB + BKP datasets. Power law baseline best fit is provided in black. Power spectra from WWI and the data, that residual from power law best fit model are plotted below to highlight the features in the angular power spectra.

data favors a low baryon density ($\Omega_b h^2 \sim 0.0222$) while E-polarization goes for a higher ($\Omega_b h^2 \sim 0.024$) value. The baseline model can not trade-off for the baryon density and hence settles for marginal worse likelihood to all datasets. We carry out the analysis with TT + TE + EE + lowTEB + BICEP-Keck-Planck dust specifically to point out the individual

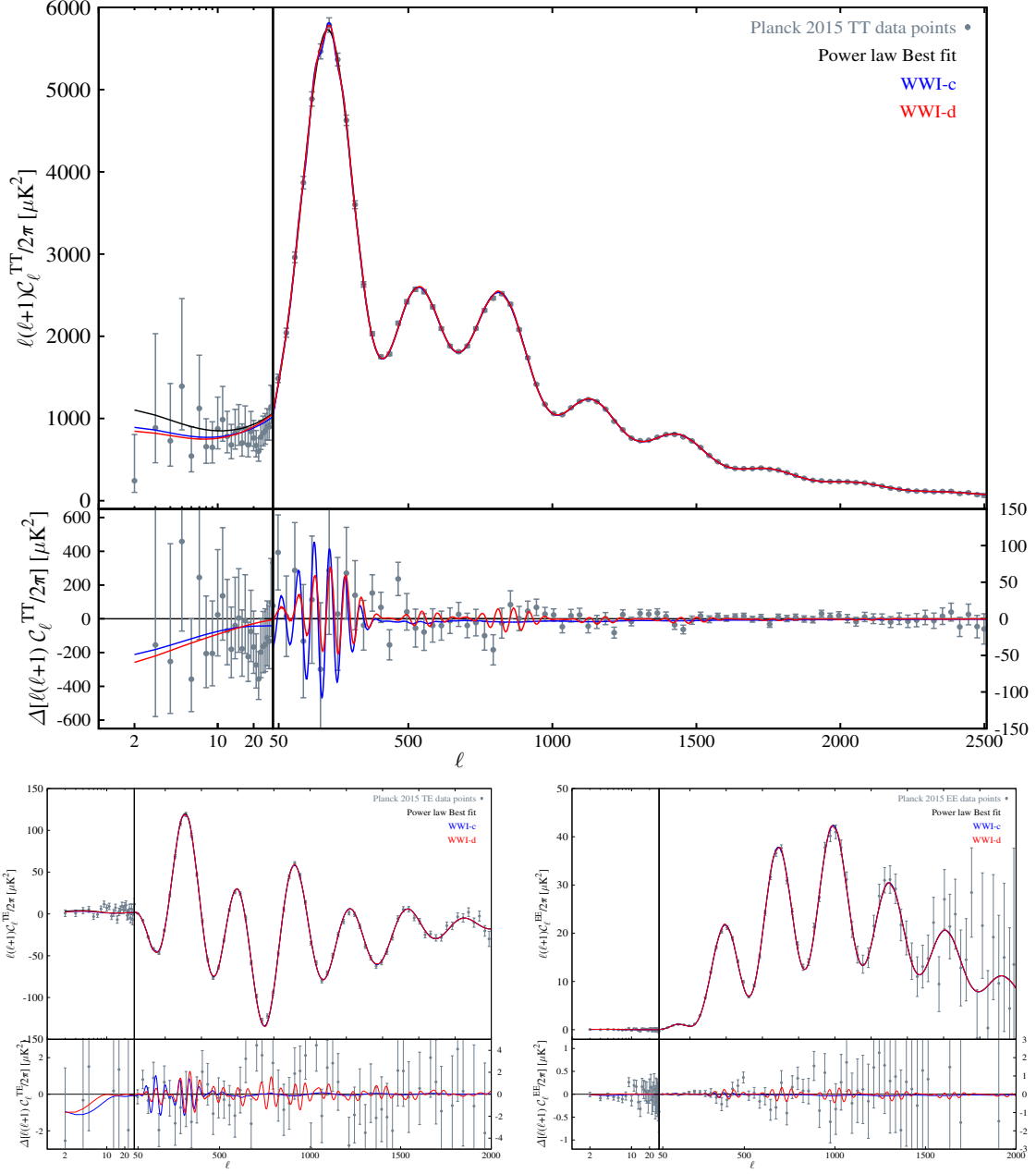


Figure 4. Wiggly Whipped Inflation : Angular power spectra for temperature and polarization anisotropies. Theoretical predictions from WWI-c and WWI-d are provided. These are the best fits to TTTEEE + lowTEB + BKP datasets. Power law baseline best fit is provided in black. Power spectra from WWI and the data, that are residual from power law best fit model are plotted below to highlight the features in the angular power spectra.

worse fits. WWI-b and WWI-d manage to compensate for the baseline worse fit by providing wiggles in the PPS that can address EE data better than the baseline model *but* at the same time keeping a low baryon density ($\Omega_b h^2 \sim 0.023$). These two spectra represent the global fit to the overall Planck data. Though the WWI-b and WWI-d are indistinguishable from

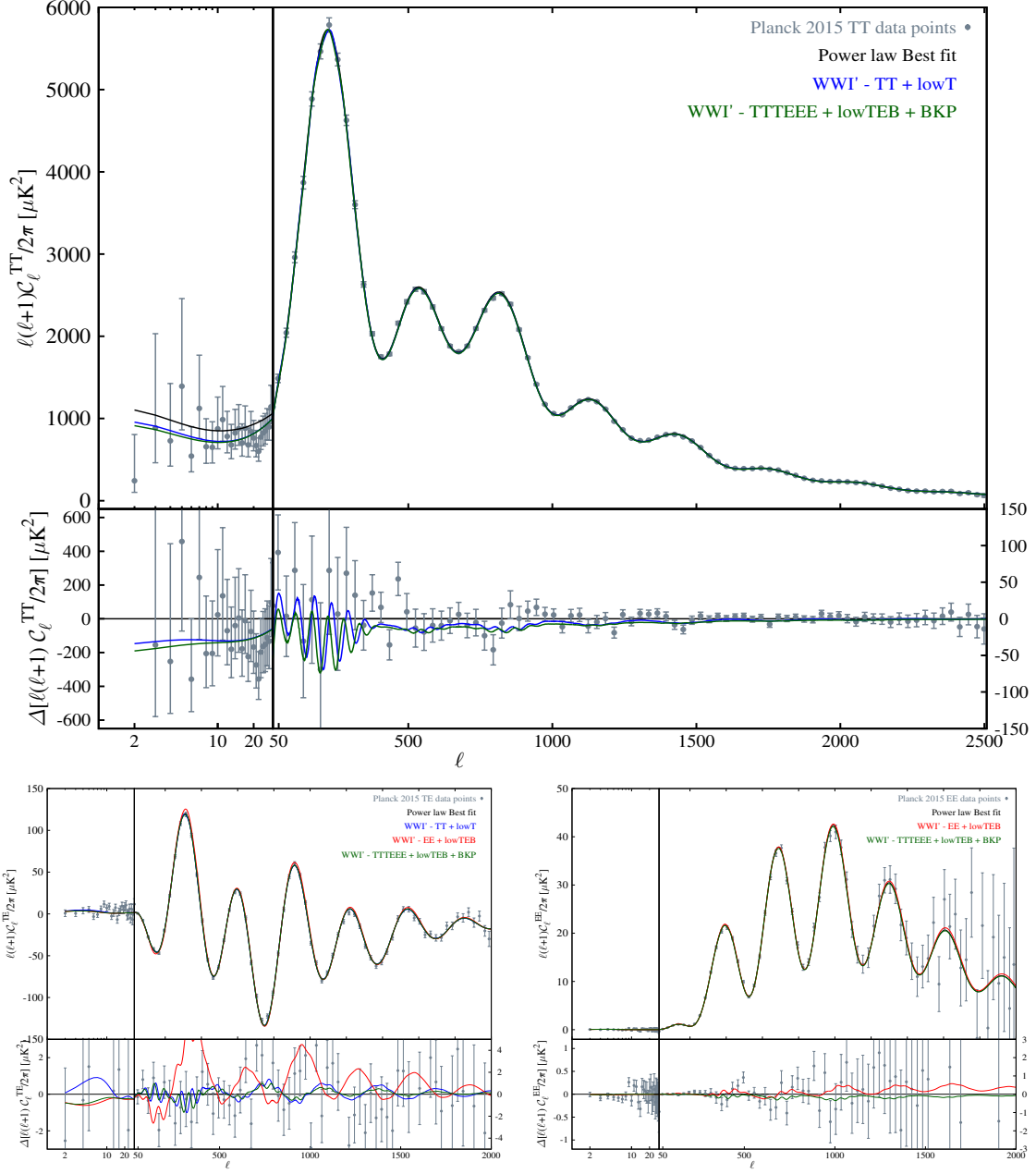


Figure 5. Wiggly Whipped Inflation : Angular power spectra for temperature and polarization anisotropies. Theoretical predictions from WWI' are provided. These are the best fits to TT + lowT, EE+lowTEB and TTTEEE + lowTEB + BKP datasets. Power law baseline best fit is provided in black. Power spectra from WWI' and the data, that are residual from power law best fit model are plotted below to highlight the features in the angular power spectra.

the likelihood values, they have distinct signatures in the power spectrum. The Wiggles in WWI-b damps down at $k \sim 0.1 \text{ Mpc}^{-1}$ while WWI-d continues to be present at smaller scales. The difference between these two spectra becomes evident when we calculate the three point correlations *i.e.* the bispectra. It is interesting that WWI', with a fixed shaped

power spectra feature, is able to provide better fit to the temperature and polarization data individually and also in combinations. In Fig. 2 (the right plot), we have provided the best fit PPS for WWI corresponding to the best fit provided in Table 1. We find $\Delta\chi^2 \sim 4$ and 6 *w.r.t.* power law when we compare WWI' with the temperature and polarization data respectively. This particular best fit do not provide better fit to the high- ℓ TT data but the best fit for EE quoted in the Table is in very good agreement with the high- ℓ EE data. However, the position and amplitude of the oscillations required to have a good agreement with TT and EE data are different. When we compare WWI' with the combined datasets, the best fit provides $\Delta\chi^2 \sim 11 - 12$ compared to power law with only 2 extra parameters. Breakdown of likelihood in temperature and polarization data is very similar to WWI-[b,d] case, and we find, WWI' with the PPS plotted in Fig. 2 is providing improvement to T and E datasets combinations from Planck since the best fit likelihoods from power law are degraded from the individual best fit values when temperature and polarization data are used separately.

In Fig. 3 and 4, we plot the best fit angular power spectra for temperature and polarization anisotropies from WWI and the Planck data. In both the plots we have also plotted the best fit results from the power law PPS in black. In each plot, the bottom panel represent the data and the power spectra residual to the power law best fit. The left panel in each plot captures the multipoles $\ell = 2 - 29$ and are plotted in log scales while the right panels display high- ℓ ($\ell = 30 - 2508$ in case of TT and $\ell = 30 - 1996$ in case of EE and TE) data and best fit results in linear scale. Note that, here the plotted results correspond to the best fit obtained against TTTEEE + lowTEB + BKP datasets. Improvement in fit from the low- ℓ data is evident the suppression in the low- ℓ residual plot in all the best fits. Only WWI-a is able to address the dip around $\ell = 22$ in a convincing manner. WWI-[b,c,d] introduce features at the high- ℓ as well. However, note that, at high- ℓ we do not get notable improvement in fit when we use temperature and polarization data separately, but in a joint analysis, WWI-b and WWI-d interestingly provide a noticeable better fit. In Fig. 5 we plot the best fit angular power spectra and their residuals from power law best fit for WWI'. Unlike WWI model, in this plot we plot best fit from TT + lowT, EE + lowTEB and TTTEEE + lowTEB + BKP. For the TT plot we show best fit from TT + lowT and TTTEEE + lowTEB + BKP and for EE plot we present EE + lowTEB and TTTEEE + lowTEB + BKP best fits. For TE, we provide all three best fit power spectra. In the TE plot, the EE best fit is seen to be not fitting the data well at the acoustic peaks. Since high- ℓ temperature data is not used in obtaining EE + lowTEB best fit, we can expect some disagreement between temperature and polarization best fits. The large mismatch here might point out a systematic tension between T and E data. However, we should note that the statistical uncertainties in the EE data is substantially larger than the TT data and differences in their best fits can just be an artifact of statistical fluctuations.

4.3 Change in the parameter constraints

The presence of features change the background parameter constraints from power law. Due to the features in WWI and WWI' we find certain changes in the background parameters. The power suppression at large angular scales shifts the reionization optical depth to a higher value $\tau \sim 0.07 - 0.1$ compared to the power law case. Here, we present only the change in the baryon density constraints. In Fig. 6, we plot the marginalized likelihoods from power law, WWI and WWI'. Note that for WWI, in arriving at the constraints, we have fixed the width of the transition (Δ) to the best fit value of WWI-d using the prior knowledge that WWI-d is able to provide an agreement to the baryon density mismatch from power law PPS. In this

figure the each plot at the top corresponds to different models that compares the difference in the likelihood of baryon density from T, E and from their combination. For power law model we note that the peak of the likelihood from EE + lowTEB is significantly far away from the tail of TT + lowT data. When feature models are used for the PPS, we find that the likelihoods shift towards lower baryon density for EE (from $\Omega_b h^2 \sim 0.024$ for power law to ~ 0.023 for WWI and WWI'). In the bottom panel of the same figure, we provide the same likelihoods but plotted for T, E and complete datasets for comparison. We find that the shift is not substantial given the large standard deviation of EE data but it definitely reduces the tension to a fair extent that amounts to 12-14 improvement in χ^2 values. Furthermore, we find that the tension is not relaxed due to the increase in degeneracy owing to the extra parameters. In fact, we find that for WWI and WWI' models, the likelihood of baryon density is sharper than the power law. The standard deviation of the likelihood in WWI and WWI' models are 0.0012 and 0.001 respectively while for power law it is 0.0014. Qualitatively the likelihoods can also be compared in middle plot of lower panel of Fig. 6. Here, we would like to point out that since our slow roll part of the potential generates a spectral tilt ~ 0.96 (the asymptotic or average n_s at small scales), in our analyses we do not have the scope of marginalizing over the spectral tilt and hence the comparison with power law case, where we marginalize over n_s , might not be complete. Hence we obtained the standard deviation of the baryon density from the power law model against EE + lowTEB dataset by fixing the $n_s = 0.964$, which turns out to be ~ 0.001 , similar to WWI' model. For the complete datasets used in the analyses, we find that the standard deviations for WWI and WWI' are similar to the power law case as well. In other words, we find tighter (or at least similar) constraints on background parameters with WWI and WWI' models as in power law model.

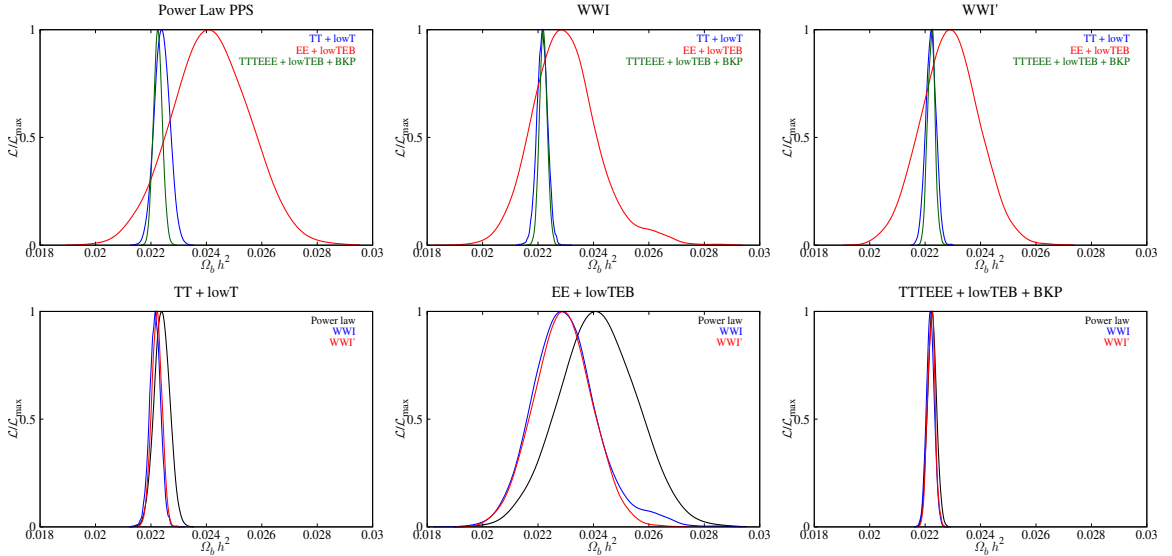


Figure 6. The likelihood of baryon density obtained from temperature and polarization data from Planck-2015. In the top panel, in each plot, we provide the likelihood obtained assuming the power law, WWI and WWI' form of inflation. Note that when we assume power law PPS, the E polarization data favors a large baryon density ($\Omega_b h^2 \sim 0.024$) which looks having slight disagreement with the temperature data. WWI and WWI' reduce this disagreement with a mean value of baryon density $\Omega_b h^2 \sim 0.023$. In the bottom panel we compare the results from different inflationary models and power law PPS for different datasets. The shift of the likelihoods to the lower baryon density is evident for WWI and WWI' models for EE + lowTEB data.

Though we are getting substantial improvement in likelihood compared to power law with both WWI and WWI', we fail to get more than 1σ evidence for these features. The maximum likelihoods show significant deviation from featureless case in both the models, but when marginalized, we find that the best fits have low marginalized probabilities. Hence, with Planck data we are unable to rule out featureless primordial power spectrum even though feature models agree with the data substantially better.

At this point we should mention that WWI-[b,c,d] and WWI' contain features around the BAO scales and hence the matter power spectra can be constrained using the large scale structure data as well. With the upcoming data from DESI [45], SDSS-IV, e-BOSS [46, 47], Euclid [48] we expect to verify the existence of these features. Also with the upcoming low- ℓ EE data from Planck HFI is supposed to provide stronger constraints on the large scale suppression. We expect to revisit Wiggly Whipped Inflation with the future datasets from CMB and LSS.

4.4 Non-Gaussianity

It has been extensively discussed in the literature that inflation models, that offers departure from slow roll inflation to generate features in the PPS, also produce non-negligible non-Gaussianities [37, 38, 49–54]. In this paper we shall only consider the three point correlations, *i.e.* the bispectra generated by WWI and WWI'. We use BINGO-2.0 [37, 38, 55] to calculate the bispectra for our best fit models. We have used the best fit potential parameters from TTTEEE + lowTEB + BKP for WWI-[a,b,c,d] and WWI' and compute the f_{NL} . We calculate all the terms contributing to the f_{NL} arising from the interaction Hamiltonian, cubic in order of the curvature perturbations [49, 53, 56]. Since WWI best fit PPS do have features with high frequency and high amplitude, any slow-roll approximation in the bispectrum integral shall underestimate the actual value of the f_{NL} . Using BINGO, we do not make any approximation and evaluate the bispectrum integral numerically. We calculate local f_{NL} for our models derived from bispectrum $\mathcal{B}_s(\mathbf{k}_1, \mathbf{k}_2, \mathbf{k}_3)$,

$$f_{\text{NL}}(\mathbf{k}_1, \mathbf{k}_2, \mathbf{k}_3) = -\frac{10}{3} (2\pi)^{-4} (2\pi)^{9/2} k_1^3 k_2^3 k_3^3 \mathcal{B}_s(\mathbf{k}_1, \mathbf{k}_2, \mathbf{k}_3) \times [k_1^3 P_s(k_2) P_s(k_3) + \text{two permutations}]^{-1}, \quad (4.1)$$

where $P_s(k)$ denotes the primordial power spectra.

In Fig. 7 we plot the f_{NL} for the best fit potentials obtained from TTTEEE + lowTEB + BKP datasets. To the left we plot the f_{NL} in equilateral limit ($k_1 = k_2 = k_3 = k$). To the right we plot the 2D heat map of the f_{NL} . The 2D f_{NL} are plotted as a function of k_3/k_1 and k_2/k_1 . The top left corner of the triangular configurations represent the squeezed limit ($k_2, k_3 \ll k_1$) and the top right corner represent the equilateral limit. k_1 in WWI-[a,b,c,d] and WWI' are chosen to be $\sim 2 \times 10^{-3}$, 0.03, 0.015, 0.14 and 0.14 Mpc^{-1} respectively. For the first three cases, we chose the mode k_1 by locating the scale where f_{NL} becomes maximum and for WWI-d and WWI' we chose it to be a smaller scale since for a sharp transition in the potential (or in its derivative in the later case), the f_{NL} is expected to diverge linearly with wavenumber and a smaller k_1 is expected to capture the profile of the f_{NL} in the 2D heat map.

Note that the WWI-a and WWI-c generates $|f_{\text{NL}}| \sim 1 - 10$. Because of the presence of a broad step in the potential and wide frequency oscillations, the slow-roll parameters $\epsilon_{i+1} = d \ln \epsilon_{i+1} / dN$ and their derivatives are not large enough to produce large three point

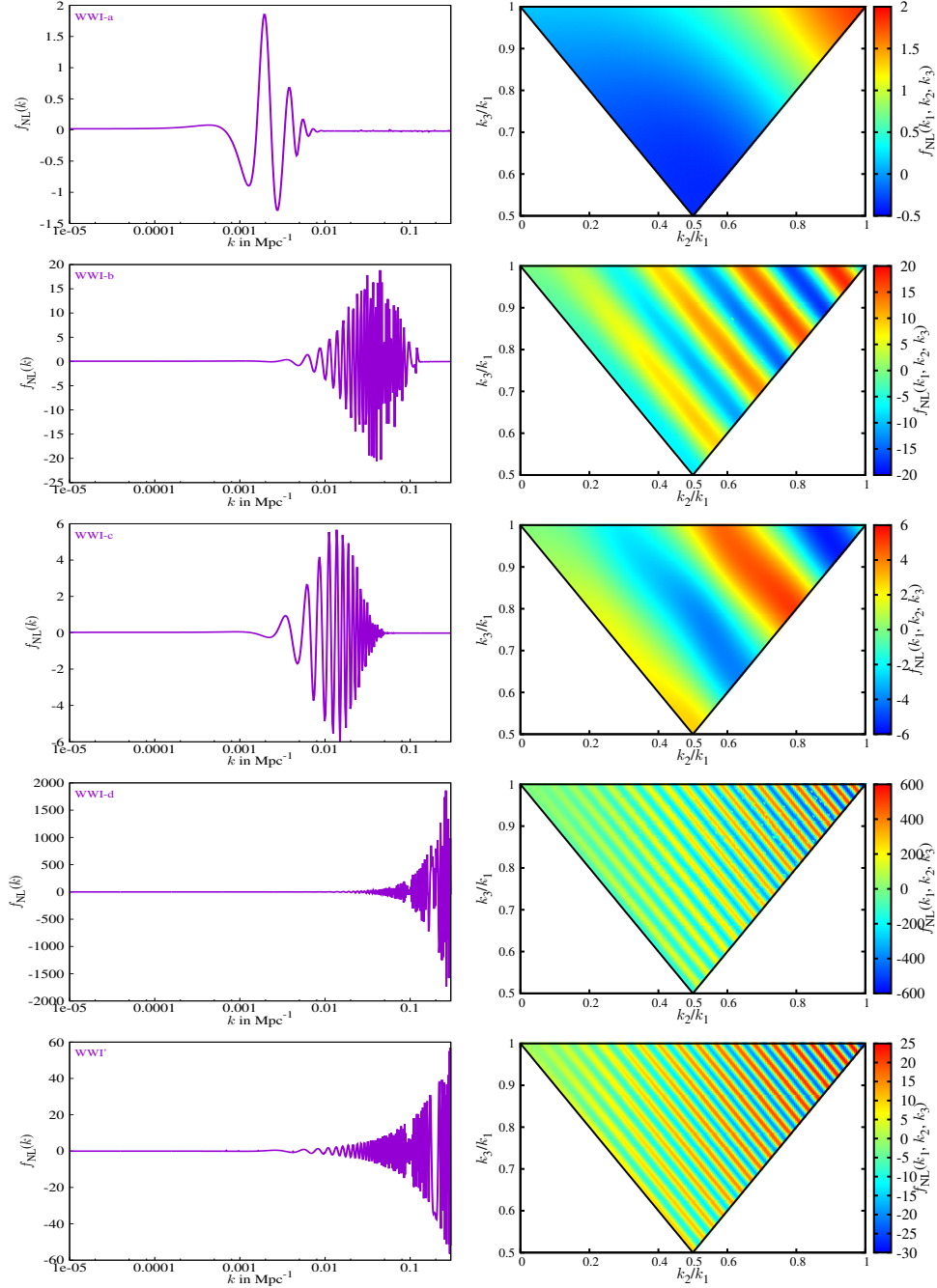


Figure 7. Wiggly Whipped Inflation : f_{NL} in equilateral (left) and in arbitrary triangular configurations (right). From top to bottom we plot the f_{NL} from WWI-a, WWI-b, WWI-c, WWI-d and WWI' respectively (see, Fig. 2 for corresponding PPS). Note that while WWI-a provides $f_{\text{NL}} \sim \mathcal{O}(1)$ which has a localized feature around $k \sim 0.002 \text{Mpc}^{-1}$, features that extend over wide range of cosmological scales with larger frequency, generate higher non-Gaussianity with $f_{\text{NL}} \sim \mathcal{O}(100 - 1000)$.

correlations of curvature perturbations. While WWI-b, WWI-d and WWI' generates higher f_{NL} because of sharper transition from moderate fast roll to slow-roll potential ($\Delta \rightarrow 0$). We would like to point a crucial difference between WWI-b and WWI-d (or WWI') models.

When we compare these two models with the temperature and polarization angular power spectrum, we find similar improvement in fit compared to power law models. Hence, to the power spectra level, these models are nearly indistinguishable. On the other hand the WWI-b generates f_{NL} which converges at small scales but WWI-d and WWI' diverges with the wavenumbers because the singularity at $\phi = \phi_{\text{T}}$ (although, note that in strict numerical sense, we have to model the singularity by a transition width very close to zero). The divergent f_{NL} arising from the instantaneous transition and the effect of smoothing the discontinuity were studied before in literature [50–52]*. As we have pointed out before, the WWI' essentially generates same power spectra as generated by Starobinsky-1992 model of inflation with a spectral tilt of ~ 0.96 . The bispectra generated from this model, hence are of same shape as discussed in literature [38, 49–52]. To evaluate the f_{NL} from the WWI' model we have used a Theta function and Delta function with a width similar to WWI-d model, to reproduce the effects of the singularity in the second derivative of the potential. We should emphasize that an instantaneous transition is not a realistic situation and there has to be a finite width associated with the transition in the potential that ensures the convergence of bispectra at small scales (as have been emphasized in [52]).

From the analyses above we can state that feature models, that are indistinguishable from the likelihood *w.r.t.* the power spectra data, a joint estimation of PPS and bispectra can quantitatively be able to distinguish between the models, and also provide extra significance for primordial features in the data, if present. There are hints of oscillatory bispectra from Planck 2015 analysis [57] and hence it is important to confront the WWI features with Planck bispectra data. We emphasize that since WWI, within its single framework, offers a wide variety of features, this model will be extremely useful in comparing different features.

5 Conclusions

In this paper we confront Wiggly Whipped inflaton potentials allowing deviations from strict slow roll, against the latest Planck 2015 angular power spectrum data of temperature and polarization and BICEP2/Keck B-mode polarization data. WWI offers a simple transition from moderate fast roll to strict slow roll potential with/without the presence of a discontinuity/jump in the potential at the field value of phase transition. We also present WWI', in which a smooth part of the inflaton potential is that of the $R + R^2$ inflationary model [27] in the Einstein frame (and which in turn represents a special case of the α -attractor model [26]) and discontinuity appears only in the first derivative of the potential. We have been able to generate a wide class of primordial features that have been discussed in the literature within the frameworks of WWI and WWI'. Owing to the flexibility of the WWI model, we are able to locate the local minima and possibly the global minima in the parameter space of WWI using only one potential. From the individual and joint analyses of T, E and B polarization we identify 4 distinguishable features in the primordial power spectra of WWI, namely WWI-[a,b,c,d]. In all the cases we notice a common pattern, the large scale suppression of scalar perturbation spectra. WWI-a provides a dip in the power spectra at $2 \times 10^{-3} \text{Mpc}^{-1}$, which has been discussed extensively in the literature and we find that this feature, apart from providing an improved fit to the low- ℓ likelihood (mostly from around $\ell = 22$), also provides better fit to high- ℓ EE datasets. We find localized oscillations (but wider than WWI-a) within $0.002 - 0.05 \text{Mpc}^{-1}$ that particularly agree with high- ℓ EE data compared to power law best fit. WWI-a and WWI-c represent the primordial features that attempts to address

*We find $\Delta \sim 10^{-3}$ for WWI-b and 10^{-5} for WWI-d

the features in the individual CMB angular power spectra data, that are not addressed by standard power law PPS. Apart from these best fits, our analysis with WWI offers a third kind of feature where the primordial power spectrum do not provide notable improvement in fit when compared with TT and EE angular power spectrum individually, but provides 12–14 improvement in fit in χ^2 compared to power law *w.r.t.* the complete dataset. Similarly in WWI', using only 2 extra parameters in the inflation potential, we find ~ 12 improvement in χ^2 fit. WWI' offers a step like suppression at larger scales accompanied by oscillations at smaller scales. In this model we show that primordial feature of a fixed shape, by changing its location and amplitude, can match both temperature, polarization data separately and also in a combined analysis. We find that the standard baseline model of cosmology prefers higher baryon density ($\Omega_b h^2 \sim 0.024$ as best fit value) for E-mode polarization which is more than 3σ away from the TT best fit. Though the uncertainties in the E-mode polarization data are much larger than temperature data and the distance to the best fit values from EE data can not be trusted in a statistically robust analysis, we demonstrated that TT, EE Likelihood decrease in a joint analysis.[†] WWI-b, WWI-d and WWI' offering high frequency oscillations extending over a large range of cosmological scales offer a scenario that fits the TT, EE, EE and lowTEB data better in joint analyses, keeping the best fit value of $\Omega_b h^2 \sim 0.0222$, as demanded by temperature power spectrum. Both WWI and WWI' show a shift in baryon density to a lower value ($\Omega_b h^2 \sim 0.023$) when compared with EE dataset. We find that WWI-b and WWI-d represent the global best fit to the complete Planck 2015 and BICEP2/KECK datasets. The fundamental difference between WWI-b and WWI-d is in the sharpness of their transition from moderate fast roll to the complete slow roll regime. These two features are indistinguishable from the angular power spectrum analyses but we show that they have very distinct bispectra signatures. It is possible to find stringent constraints on the WWI and WWI' models upon joint analyses with CMB power spectra and bispectra data.

Acknowledgments

DKH and GFS acknowledges Laboratoire APC-PCCP, Université Paris Diderot and Sorbonne Paris Cité (DXCACHEXGS) and also the financial support of the UnivEarthS Labex program at Sorbonne Paris Cité (ANR-10-LABX-0023 and ANR-11-IDEX-0005-02). DKH would like to thank the hospitality of Cluster Computing Center (through the support from the DOE HEP's Forum on Computational Excellence) and Berkeley Center for Cosmological Physics, LBL, Berkeley and Princeton University where a part of the work has been carried out. AS would like to acknowledge the support of the National Research Foundation of Korea (NRF-2013R1A1A2013795). AAS was partially supported by the grant RFBR 14-02-00894 and by the Russian Government Program of Competitive Growth of Kazan Federal University.

References

- [1] N. Aghanim *et al.* [Planck Collaboration], [arXiv:1507.02704 [astro-ph.CO]].
- [2] P. A. R. Ade *et al.* [Planck Collaboration], arXiv:1502.01589 [astro-ph.CO].
- [3] See, <http://www.cosmos.esa.int/web/planck/pla>.

[†]Here we would like to mention that this difference can also be an artifact of the systematics in the Planck polarization and temperature data [58]

- [4] H. V. Peiris *et al.* [WMAP Collaboration], *Astrophys. J. Suppl.* **148**, 213 (2003) [astro-ph/0302225].
- [5] E. Komatsu *et al.* [WMAP Collaboration], *Astrophys. J. Suppl.* **180**, 330 (2009) doi:10.1088/0067-0049/180/2/330 [arXiv:0803.0547 [astro-ph]].
- [6] E. Komatsu *et al.* [WMAP Collaboration], *Astrophys. J. Suppl.* **192**, 18 (2011) doi:10.1088/0067-0049/192/2/18 [arXiv:1001.4538 [astro-ph.CO]].
- [7] G. Hinshaw *et al.* [WMAP Collaboration], *Astrophys. J. Suppl.* **208**, 19 (2013) doi:10.1088/0067-0049/208/2/19 [arXiv:1212.5226 [astro-ph.CO]].
- [8] P. A. R. Ade *et al.* [Planck Collaboration], arXiv:1303.5082 [astro-ph.CO].
- [9] P. A. R. Ade *et al.* [Planck Collaboration], arXiv:1502.02114 [astro-ph.CO].
- [10] D. K. Hazra, A. Shafieloo and T. Souradeep, *JCAP* **1411**, no. 11, 011 (2014) doi:10.1088/1475-7516/2014/11/011 [arXiv:1406.4827 [astro-ph.CO]].
- [11] P. A. R. Ade *et al.* [BICEP2 Collaboration], arXiv:1403.4302 [astro-ph.CO].
- [12] P. A. R. Ade *et al.* [BICEP2 Collaboration], arXiv:1403.3985 [astro-ph.CO].
- [13] D. K. Hazra, A. Shafieloo, G. F. Smoot and A. A. Starobinsky, *JCAP* **1406**, 061 (2014) doi:10.1088/1475-7516/2014/06/061 [arXiv:1403.7786 [astro-ph.CO]].
- [14] D. K. Hazra, A. Shafieloo and G. F. Smoot, *JCAP* **1312**, 035 (2013) arXiv:1310.3038 [astro-ph.CO].
- [15] D. K. Hazra, A. Shafieloo, G. F. Smoot and A. A. Starobinsky, *Phys. Rev. Lett.* **113**, no. 7, 071301 (2014) doi:10.1103/PhysRevLett.113.071301 [arXiv:1404.0360 [astro-ph.CO]].
- [16] D. K. Hazra, A. Shafieloo, G. F. Smoot and A. A. Starobinsky, *JCAP* **1408**, 048 (2014) doi:10.1088/1475-7516/2014/08/048 [arXiv:1405.2012 [astro-ph.CO]].
- [17] P. A. R. Ade *et al.* [BICEP2 and Planck Collaborations], *Phys. Rev. Lett.* **114**, 101301 (2015) doi:10.1103/PhysRevLett.114.101301 [arXiv:1502.00612 [astro-ph.CO]].
- [18] P. A. R. Ade *et al.* [BICEP2 and Keck Array Collaborations], *Phys. Rev. Lett.* **116**, 031302 (2016) doi:10.1103/PhysRevLett.116.031302 [arXiv:1510.09217 [astro-ph.CO]].
- [19] A. A. Starobinsky, *JETP Lett.* **55**, 489 (1992).
- [20] A. D. Linde, *Phys. Rev. D* **59**, 023503 (1999) [hep-ph/9807493].
- [21] A. D. Linde, M. Sasaki and T. Tanaka, *Phys. Rev. D* **59**, 123522 (1999) [astro-ph/9901135].
- [22] M. Joy, V. Sahni, A. A. Starobinsky, *Phys. Rev. D* **77**, 023514 (2008) [arXiv:0711.1585].
- [23] M. Joy, A. Shafieloo, V. Sahni, A. A. Starobinsky, *JCAP* **0906**, 028 (2009) [arXiv:0807.3334].
- [24] R. Bousso, D. Harlow and L. Senatore, arXiv:1309.4060 [hep-th].
- [25] C. R. Contaldi, M. Peloso, L. Kofman and A. D. Linde, *JCAP* **0307**, 002 (2003) [astro-ph/0303636].
- [26] R. Kallosh and A. Linde, *JCAP* **1307**, 002 (2013) doi:10.1088/1475-7516/2013/07/002 [arXiv:1306.5220 [hep-th]]; R. Kallosh and A. Linde, *JCAP* **1312**, 006 (2013) doi:10.1088/1475-7516/2013/12/006 [arXiv:1309.2015 [hep-th]]; R. Kallosh, A. Linde and D. Roest, *JHEP* **1311**, 198 (2013) doi:10.1007/JHEP11(2013)198 [arXiv:1311.0472 [hep-th]].
- [27] A. A. Starobinsky, *Phys. Lett. B* **91**, 99 (1980). doi:10.1016/0370-2693(80)90670-X
- [28] G. Efstathiou and S. Chongchitnan, *Prog. Theor. Phys. Suppl.* **163**, 204 (2006) doi:10.1143/PTPS.163.204 [astro-ph/0603118].
- [29] D. K. Hazra, M. Aich, R. K. Jain, L. Sriramkumar and T. Souradeep, *JCAP* **1010**, 008 (2010) [arXiv:1005.2175 [astro-ph.CO]].

- [30] S. Hannestad, Phys. Rev. D **63** (2001) 043009 [astro-ph/0009296]; M. Tegmark and M. Zaldarriaga, Phys. Rev. D **66** (2002) 103508 [astro-ph/0207047]; S. L. Bridle, A. M. Lewis, J. Weller and G. Efstathiou, Mon. Not. Roy. Astron. Soc. **342** (2003) L72 [astro-ph/0302306]; P. Mukherjee and Y. Wang, Astrophys. J. **599** (2003) 1 [astro-ph/0303211]; D. Tocchini-Valentini, Y. Hoffman and J. Silk, Mon. Not. Roy. Astron. Soc. **367** (2006) 1095 [astro-ph/0509478]; N. Kogo, M. Sasaki and J. 'i. Yokoyama, Prog. Theor. Phys. **114** (2005) 555 [astro-ph/0504471]; S. M. Leach, Mon. Not. Roy. Astron. Soc. **372** (2006) 646 [astro-ph/0506390]; A. Shafieloo and T. Souradeep, Phys. Rev. D **78** (2008) 023511 [arXiv:0709.1944 [astro-ph]]; P. Paykari and A. H. Jaffe, Astrophys. J. **711** (2010) 1 [arXiv:0902.4399 [astro-ph.CO]]; G. Nicholson and C. R. Contaldi, JCAP **0907**, 011 (2009) [arXiv:0903.1106 [astro-ph.CO]]; C. Gauthier and M. Bucher, JCAP **1210**, 050 (2012) [arXiv:1209.2147 [astro-ph.CO]]; R. Hlozek, J. Dunkley, G. Addison, J. W. Appel, J. R. Bond, C. S. Carvalho, S. Das and M. Devlin *et al.*, Astrophys. J. **749** (2012) 90 [arXiv:1105.4887 [astro-ph.CO]]; J. A. Vazquez, M. Bridges, M. P. Hobson and A. N. Lasenby, JCAP **1206**, 006 (2012) [arXiv:1203.1252 [astro-ph.CO]]; D. K. Hazra, A. Shafieloo and T. Souradeep, JCAP **1307**, 031 (2013) [arXiv:1303.4143 [astro-ph.CO]]; D. K. Hazra, A. Shafieloo and T. Souradeep, Phys. Rev. D **87**, 123528 (2013) [arXiv:1303.5336 [astro-ph.CO]]; P. Hunt and S. Sarkar, arXiv:1308.2317 [astro-ph.CO]; S. Dorn, E. Ramirez, K. E. Kunze, S. Hofmann and T. A. Ensslin, JCAP **1406**, 048 (2014) [arXiv:1403.5067 [astro-ph.CO]].
- [31] A. Shafieloo and T. Souradeep, Phys. Rev. D **70** (2004) 043523 [astro-ph/0312174].
- [32] R. Bouso, D. Harlow and L. Senatore, arXiv:1404.2278 [astro-ph.CO].
- [33] R. Allahverdi, K. Enqvist, J. Garcia-Bellido and A. Mazumdar, Phys. Rev. Lett. **97** (2006) 191304 [hep-ph/0605035]; R. K. Jain, P. Chingangbam, J. -O. Gong, L. Sriramkumar and T. Souradeep, JCAP **0901** (2009) 009 [arXiv:0809.3915 [astro-ph]].
- [34] B. A. Powell and W. H. Kinney, Phys. Rev. D **76**, 063512 (2007) doi:10.1103/PhysRevD.76.063512 [astro-ph/0612006].
- [35] J. A. Adams, B. Cresswell and R. Easther, Phys. Rev. D **64** (2001) 123514 [astro-ph/0102236]; L. Covi, J. Hamann, A. Melchiorri, A. Slosar and I. Sorbera, Phys. Rev. D **74** (2006) 083509 [astro-ph/0606452]; M. J. Mortonson, C. Dvorkin, H. V. Peiris and W. Hu, Phys. Rev. D **79** (2009) 103519 [arXiv:0903.4920 [astro-ph.CO]]; V. Miranda, W. Hu and P. Adshead, Phys. Rev. D **86**, 063529 (2012) [arXiv:1207.2186 [astro-ph.CO]]; M. Benetti, arXiv:1308.6406 [astro-ph.CO]; A. E. Romano and A. G. Cadavid, arXiv:1404.2985 [astro-ph.CO].
- [36] T. Biswas, A. Mazumdar and A. Shafieloo, Phys. Rev. D **82**, 123517 (2010) [arXiv:1003.3206 [hep-th]]; R. Flauger, L. McAllister, E. Pajer, A. Westphal and G. Xu, JCAP **1006**, 009 (2010) [arXiv:0907.2916 [hep-th]]; C. Pahud, M. Kamionkowski and A. R. Liddle, Phys. Rev. D **79**, 083503 (2009) doi:10.1103/PhysRevD.79.083503 [arXiv:0807.0322 [astro-ph]]; M. Aich, D. K. Hazra, L. Sriramkumar and T. Souradeep, Phys. Rev. D **87**, 083526 (2013) [arXiv:1106.2798 [astro-ph.CO]]; D. K. Hazra, JCAP **1303**, 003 (2013) [arXiv:1210.7170 [astro-ph.CO]]; H. Peiris, R. Easther and R. Flauger, arXiv:1303.2616 [astro-ph.CO]; P. D. Meerburg and D. N. Spergel, Phys. Rev. D **89**, 063537 (2014) [arXiv:1308.3705 [astro-ph.CO]]; R. Easther and R. Flauger, arXiv:1308.3736 [astro-ph.CO].
- [37] D. K. Hazra, L. Sriramkumar and J. Martin, JCAP **1305**, 026 (2013) [arXiv:1201.0926 [astro-ph.CO]].
- [38] V. Sreenath, D. K. Hazra and L. Sriramkumar, JCAP **1502**, no. 02, 029 (2015) doi:10.1088/1475-7516/2015/02/029 [arXiv:1410.0252 [astro-ph.CO]].
- [39] See, <http://camb.info/>.
- [40] A. Lewis, A. Challinor and A. Lasenby, Astrophys. J. **538** (2000) 473 [astro-ph/9911177].
- [41] See, <http://cosmologist.info/cosmomc/>.

- [42] A. Lewis and S. Bridle, Phys. Rev. D **66** (2002) 103511 [astro-ph/0205436].
- [43] M. J. D. Powell, Cambridge NA Report NA2009/06, University of Cambridge, Cambridge (2009).
- [44] See,
http://wiki.cosmos.esa.int/planckpla2015/index.php/CMB_spectrum_%26_Likelihood_Code.
- [45] See <http://desi.lbl.gov>.
- [46] See <http://www.sdss.org/surveys>.
- [47] See <http://www.sdss.org/surveys/eboss/>.
- [48] See <http://www.euclid-ec.org/>.
- [49] J. Martin and L. Sriramkumar, JCAP **1201**, 008 (2012) [arXiv:1109.5838 [astro-ph.CO]].
- [50] F. Arroja, A. E. Romano and M. Sasaki, Phys. Rev. D **84**, 123503 (2011) [arXiv:1106.5384 [astro-ph.CO]].
- [51] F. Arroja and M. Sasaki, JCAP **1208**, 012 (2012) [arXiv:1204.6489 [astro-ph.CO]].
- [52] J. Martin, L. Sriramkumar and D. K. Hazra, JCAP **1409**, no. 09, 039 (2014) doi:10.1088/1475-7516/2014/09/039 [arXiv:1404.6093 [astro-ph.CO]].
- [53] X. Chen, Adv. Astron. **2010**, 638979 (2010); X. Chen, R. Easther and E. A. Lim, JCAP **0706**, 023 (2007); JCAP **0804**, 010 (2008).
- [54] R. Flauger and E. Pajer, JCAP **1101**, 017 (2011) doi:10.1088/1475-7516/2011/01/017 [arXiv:1002.0833 [hep-th]].
- [55] See <https://sites.google.com/site/codecosmo/bingo>.
- [56] J. Maldacena, JHEP **0305**, 013 (2003).
- [57] P. A. R. Ade *et al.* [Planck Collaboration], arXiv:1502.01592 [astro-ph.CO].
- [58] G. E. Addison, Y. Huang, D. J. Watts, C. L. Bennett, M. Halpern, G. Hinshaw and J. L. Weiland, Astrophys. J. **818**, no. 2, 132 (2016) doi:10.3847/0004-637X/818/2/132 [arXiv:1511.00055 [astro-ph.CO]].